Contents list available at CBIORE journal website

International Journal of Renewable Energy Development

Journal homepage: https://ijred.cbiore.id

Research Article

Development of FeCo/C and AgFeCo/C cathode catalysts for xylitol membraneless alkaline fuel cells

Supansa Dampat[a], Sonchai Intachai[a], Bancha Yingngam[b], Chakkrapong Chaiburi[c]*

[a]*Department of Physical Sciences, Faculty of Science and Digital Innovation, Thaksin University, Phatthalung Campus, Papayom District, Phatthalung Province, 93210, Thailand*

[b]*Faculty of Pharmaceutical Sciences, Ubon Ratchathani University, 85 Sathonlamark Road, Warin Chamrap District, Ubon Ratchathani Province, 34190, Thailand*

[c]*Faculty of Engineering, Thaksin University, Phatthalung Campus, Papayom District, Phatthalung Province, 93210, Thailand*

Abstract. In the study, researchers developed and characterized xylitol membraneless alkaline fuel cell catalysts—namely FeCo/C, AgFeCo/C, and Pd/C—for cathodes and anodes. The first part of our investigation details the catalysts' morphology and elemental composition. STEM, EDS, and EDS mapping confirmed that the catalysts exhibited a small, lumpy structure, with the alloy well-dispersed across the support material. The X-ray diffraction pattern for the cathode catalyst reveals that the spectral lines corresponding to the Ag metal peak at a 2θ maximum of 38.12 degrees exhibit a 111 pattern, suggesting the existence of Ag metal particles in a face-centered cubic (fcc) arrangement. Meanwhile, the metal peaks for Fe_3O_4 and Co_3O_4 appear at maximum 2θ positions of 35.45 and 30.09 degrees, respectively, displaying 311 and 220 patterns, which indicate the presence of Fe_3O_4 and Co_3O_4 particles with spinel cubic structures. In the case of the anode catalyst, the spectral line for the Pd metal peak at a 2θ maximum of 40.12 degrees shows a 111 pattern, confirming the presence of Pd metal particles with a face-centered cubic (fcc) structure. Second, to determine the electrocatalytic properties, cyclic voltammetry (CV) measurements were conducted with xylitol as the fuel, utilizing concentrations between 0.1 and 0.5 M in 0.1 M KOH. For the cathode-side FeCo/C and AgFeCo/C catalysts, oxidation resistance was observed, and the reduction reaction diminished with increasing xylitol concentration, attributed to interfering non-conductive hydrocarbons. Conversely, Pd/C catalysts exhibited remarkable catalytic performance, particularly at 0.1 M xylitol solution, where the oxidation peak current density reached a maximum of 0.9 $mA \cdot cm^{-2}$ at -0.09 V. Finally, the researchers reported that the Pd/C-AgFeCo/C catalyst achieved the highest current density of 0.36 $A \cdot m^{-2}$ and a maximum power density of 0.129 $W \cdot m^{-2}$ for xylitol fuel cell applications.

Keywords: Alkaline, Cathode, Anode, Catalyst, Xylitol, Fuel Cell

Received: 13th March 2025; Revised: 26th May 2025; Accepted: 10th June 2025 Available online: 26th June 2025

1. Introduction

The growing adoption of renewable energy sources is a critical response to the escalating global energy crisis, which is closely linked to environmental degradation caused by increased energy demand. Among the most promising innovations in sustainable energy systems are clean energy storage and conversion technologies, including salt-based batteries and supercapacitors, as well as advanced fuel cells (Yang *et al.*, 2018). Fuel cells, in particular, stand out for their ability to continuously convert chemical energy into electricity with superior energy conversion efficiency compared to conventional methods, provided a constant fuel supply is maintained (Cruz-Reyes *et al.*, 2020). Various types of fuel cells have been developed, each exhibiting different levels of performance, with alkaline fuel cells emerging as especially promising. As Ferriday *et al.* (Ferriday *et al.*, 2021) note, alkaline fuel cells utilizing KOH electrolytes demonstrate notably higher oxygen reduction reaction rates than their acidic counterparts, especially at concentrations between 30–45 wt%, resulting in enhanced energy efficiency. Moreover, their environmental impact is minimal due to low pollutant emissions, and they offer practical advantages in terms of material storage and transportability, making them a viable component in the pursuit of cleaner, more sustainable energy systems (Wang *et al.*, 2018).

Recent research has increasingly focused on identifying alternative catalysts to replace costly and scarce platinum-group metals in fuel cell applications (Suwanraksa *et al.*, 2021). A widely supported strategy involves synthesizing various catalysts to enhance electrocatalytic performance, with particular attention to factors such as cost-effectiveness, material abundance, and structural properties conducive to electron transfer. Transition metals involving Ag, Co, Cu, Fe, Ni, and Pd are of particular interest due to their favorable surface area characteristics, which support efficient electrochemical reactions (Chutia *et al.*, 2022). Various researchers have examined the use of catalysts with different supports, including nickel cobalt on activated carbon support (Gao *et al.*, 2018), N-doped graphitic carbon shell-encapsulated FeCo (Liu *et al.*, 2021), cobalt-cerium oxide on carbon supports (Ghouri *et al.*,

* Corresponding author
Email: chakkrapong@tsu.ac.th (S. Dampat)

https://doi.org/10.61435/ijred.2025.61196
ISSN: 2252-4940/© 2025. The Author(s). Published by CBIORE

2015), palladium-nickel on carbon support electrocatalysts (López-Coronel *et al.*, 2020), and palladium-silver nickel on carbon support electrocatalysts (Elsheikh *et al.*, 2021). Fuel cell efficiency has been shown to depend largely upon the fuel type employed. In many cases, the fuels used comprise liquid fuels via direct feed, including methanol, ethanol, glycerol, and glucose, which are attractive due to their relatively low cost. Furthermore, such fuels can be produced biologically and, as such, represent a renewable source of energy (Suwanraksa *et al.*, 2022).

To evaluate non-platinum catalysts in comparison with commercially available noble metal counterparts, Kruusenberg *et al.* (Kruusenberg *et al.*, 2012) developed membrane-electrode assemblies (MEAs) utilizing a Tokuyama anion exchange membrane and focused specifically on cobalt and iron phthalocyanine catalysts supported on multi-walled carbon nanotubes (MWCNTs). Using rotating disk electrodes in a 0.1 M KOH solution, the study analyzed oxygen reduction reaction (ORR) kinetics and found that cobalt phthalocyanine electrodes achieved higher current densities than their iron-based equivalents, indicating superior electrocatalytic performance. Meanwhile, direct alkaline alcohol fuel cells were examined by Matsuoka *et al.* (Matsuoka *et al.*, 2005) using an OH-shaped anion exchange membrane and a polyhydric alcohol. The particular focus of their work was the membrane, which has the role of promoting OH ion movement to enable the fuel cell to function effectively. It was found that cells which made use of Pt–Ru/C (anode) and Pt/C (cathode) at 323 K produced 800 mV, which was in the range of 100–200 mV greater than achieved by DMFCs using Nafion®. Alkaline fuel cells can be produced using silver catalysts as cathode catalysts due to the inactivity of silver catalysts during the oxidation of polyhydrogen alcohols. For instance, the excellent performance of alkaline direct ethyl glycol fuel cells employing silver as the cathode catalyst can be attributed to the high fuel concentrations received by the anode.

In another study, Daşdelen *et al.* (Daşdelen *et al.*, 2021) explored the use of fumed silica (FS), reduced graphene oxide (rGO), and their hybrid (FS-rGO) to support gold nanoparticles in producing anode catalysts for sorbitol fuel cells. It was found that Au@FS-rGO was highly effective, offering the greatest current density for sorbitol oxidation. Catalytic activity and stability were improved by FS, which performed better than rGO, which is often employed as the support in studies of fuel cells. Weiss *et al.* (Weiss *et al.*, 2020) investigated durability and stability when using Fe-N-C electrocatalysts along with oxygen reduction reaction catalysts (ORRs). The key degradation mechanisms associated with active site demetalization and carbon corrosion are also examined, since these quickly result in an initial loss of performance, demonstrating the important role of H_2O_2 radicals as the catalysts degrade. The latest advances in Fe-N-C electrocatalysts are also explained, along with a number of suggested measures which could be taken to achieve further advances in the areas of competitive stability and sustainability.

In the work of Xu *et al.* (Xu *et al.*, 2024), it was necessary to find efficient and affordable electrocatalysts which might offer a long lifespan to upgrade the slow kinetics of the oxygen reduction reaction (ORR), which will be essential if fuel cell technologies are to be developed further. In the current study, we present dual metal single-atom catalysts (SACs) based on a metal-organic framework, namely Zn/Co−N−C, incorporating the local structures $Co-N_4$ and $Zn-N_4$. The ORR performance of these catalysts was outstanding, achieving a half-wave potential ($E_{1/2}$) of 0.938 V in relation to the reversible hydrogen electrode (RHE), while stability was largely maintained ($\Delta E_{1/2}$ = −8.5 mV) even upon reaching 50,000 electrochemical cycles. These results were obtained under the normal fuel cell operating conditions, where the peak power density achieved was around 1 $W.cm^{-2}$, which represents a new high for tested SACs in the context of alkaline fuel cells. In other work, Ho *et al.* (Ho *et al.*, 2021) studied $CoMn_2O_4$/NC nanocomposites produced through ionothermal synthesis to assess their performance as electrocatalysts for the oxygen reduction reaction in a direct glucose alkaline fuel cell (DGAFC). An ionic liquid was used to synthesize the $CoMn_2O_4$ spinel with the support of N-doped carbon. The resulting nanocomposite exhibited excellent electrocatalytic performance in the ORR, with a half-wave potential of 0.81 V (vs. RHE) while the peak diffusion-limiting current density measured 5.2 $mA.cm^{-2}$, which is not dissimilar to the performance of the commercially available Pt/C catalyst ($E_{1/2}$ vs. 0.83 V vs. RHE, Jd ≈ 5.0 $mA.cm^{-2}$). Furthermore, the catalytic performance of $CoMn_2O_4$/NC was also examined in the DGFC, in which a fuel cell which had a $CoMn_2O_4$/NC air cathode reached its peak power density at 23.72 $W.m^{-2}$.

In the work of Hu *et al.* (Hu *et al.*, 2022), glucose fuel cells (GFCs) which made use of abiotic catalysts were the focus, since these appear to provide a means of developing wearable or portable devices capable of utilizing green energy. The research explained the creation of a CoO_x-integrated carbon nanofiber (CoO_x@CNF) catalyst incorporating cobalt oxides of mixed valences which were produced via the partial oxidation of pyrolyzed electrospun Co^{2+}/polyacrylonitrile fibers. Oxidation of the pyrolyzed fibers allows modulation of the cobalt valence. Alternatively, this can be achieved by changing the ratio of cobalt acetate in the precursors. Electrocatalytic testing demonstrates that the addition of CoO to CoO_x@CNF has the effect of enhancing electrocatalytic performance because the number of available active sites for glucose electrooxidation is increased. The glucose fuel cell utilizing the CoO_x@CNF anode, comprising CoO and Co_3O_4, generated a maximum power density of 270 μ $W.cm^{-2}$, which represented an improvement in performance over that of previously reported Co_3O_4-based GFCs. The synthesis of nitrogen (N), sulfur (S), and transition metal (Ni, Co, and Fe) co-doped reduced graphene oxide (rGO) nanocomposites was performed by Dai *et al.* (Dai *et al.*, 2021) using a basic single-step *in situ* hydrothermal technique. One of the prepared materials, rGO-NS-Ni, was the catalyst which demonstrated the greatest electrochemical activity for glucose oxidation. In a direct glucose alkaline fuel cell, rGO-NS-Ni served as the anode catalyst and produced a current density measuring 148.0 $mA.cm^{-2}$, while the peak power density reached 48 W m^{-2}. Meanwhile, Suzuki *et al.* (Suzuki *et al.*, 2023) produced a fuel cell catalyst from nickel wire mesh which was coated with palladium. This required a solution of palladium chloride in water to be mixed with sodium dodecyl sulfate, which serves as an anionic surfactant to assist in the distribution of the palladium coating. The fuel cell was then assembled in a plastic container via the sequential layering of a potassium hydroxide solution, glucose, a nickel wire mesh with the palladium catalyst coating, a cellophane membrane, and a second nickel wire mesh coated with the palladium catalyst. It takes around half an hour to produce the fuel cell using this approach, which is much faster than the traditional approaches. Huang *et al.* (Huang *et al.*, 2021) investigated the oxidation of D-glucose in neutral electrolytes using a platinum catalyst, with the intention of finding applications in the field of implantable energy systems. The proposed reaction mechanism based upon the analysis of the mass changes recorded from the electrochemical measurements suggested a pair of potential pathways for oxidation. These were direct oxidation and oxidation via OH adsorption. The solvothermal method was employed to synthesize PtPd and Pt_2Pd using an anode

electrocatalyst. The maximum power density for the resulting PtPd catalyst was of 27.6 μW.cm^{-2}.

The work of Xu *et al.* (Xu *et al*., 2023) focused upon the glucose oxidation reaction, which is the main rate-limiting step of abiotic glucose fuel cells (GFCs), and the need for long-term catalysts offering a high degree of catalytic activity and oxygen resistance. It has been possible to synthesize a novel three-dimensional nitrogen-doped porous carbon material (NCZIF-8) derived from ZIF-8 to serve as catalyst support, which has a remarkable surface area measuring 944 m².g^{-1}. NCZIF-8 is supported by platinum nanoparticles (Pt NPs) which are reduced *in situ*, with a low loading 10 wt% (10% Pt/NCZIF-8). The support allows Pt NPs to be equally distributed, and makes the catalyst more durable because the nanoparticles are less likely to accumulate. Moreover, when the electrocatalytic oxidation of glucose takes place, catalytic efficiency is significantly enhanced by the greater availability of Pt active sites. NCZIF-8 is also highly porous, facilitating rapid glucose transport, while the Pt nanoparticles within the pores tend to limit the influence of oxygen upon the oxidation reaction. A 300-cycle cyclic voltammetry (CV) test revealed a very small reduction of just 7.83% in the peak current density for the 10% Pt/NCZIF-8-modified anode, which suggests a high level of durability. A novel tertiary nanocatalyst containing platinum along with nickel cobalt oxide ($NiCo_2O_4$) and reduced graphene oxide (rGO) was investigated by Askari *et al.* (Askari *et al*., 2022). This nanocatalyst was found to be very effective in catalyzing sorbitol oxidation in fuel cells. Moreover, a number of other catalysts have been synthesized, including $NiCo_2O_4$, $NiCo_2O_4$-rGO, and $NiCo_2O_4$/Pt, and their performances compared. The SOR performance was examined in the case of these nanocatalysts at a scan rate of 10 mV.s^{-1}, whereby the greatest current density was produced by $NiCo_2O_4$-rGO/Pt at 57.2 mA. cm^{-2}. Furthermore, $NiCo_2O_4$-rGO/Pt also generated the lowest peak potential at 0.64 V and exhibited superior cyclic stability when compared to other materials. Meanwhile, the work of Basu *et al.* (Basu *et al*., 2010) focused upon direct glucose fuel cells and their potential to provide power for portable low-power devices. Cyclic voltammetry in an alkaline environment was conducted in performing the electro-oxidation of glucose and fructose on a PtRu/C catalyst, with the goal of gaining insights into the factors which serve to deactivate glucose fuel cells. Testing made use of a basic DGFC in which PtRu/C served as the anode while activated coal was used as the cathode. The aim was to establish the outcomes when using different concentrations of glucose and KOH, at a range of temperatures. For a 0.3 M glucose solution in 1 M KOH, a value of 0.91 V was recorded for the open circuit voltage (OCV), which subsequently increased as the concentration of glucose increased. Peak power density was maximized at 1.38 mW.cm^{-2} when using 0.2 M glucose in 1 M KOH at a temperature of 30°C, but this value started to fall as the glucose concentration and temperature rose. Anticipating a decline in performance when switching from glucose to fructose, further testing was performed with 0.2 M fructose in 1 M KOH, which achieved a peak power density measuring 0.57 mW.cm^{-2}. The DGFC was operated for a period of 260 hours maintaining a steady load of 500 Ω, to produce a final voltage of 0.21 V. The work of Liu (Liu, 2022), however, primarily examined glucose, due to its importance as a source of energy for a majority of life forms. Glucose fuel cells are of interest to researchers since they are renewable, readily available due to their abundance, non-toxic,, inexpensive, and easily stored. Moreover, work continues with the aim of improving GFC performance. We have the aim to present a review of the literature in combination with a discussion of the technical aspects of both GFCs and membranes via the application of bibliometrics, seeking to inspire researchers to address the key challenges presented in this field in order to develop GFCs capable of superior performance. Torres-Pacheco *et al.* (Torres-Pacheco *et al*., 2020) conducted research involving sorbitol and its electrocatalytic oxidation. Sorbitol is an industrial polyalcohol which offers potential for applications in fuel cells, so this work is important in establishing an understanding of its electrochemical behavior. The synthesis of monometallic nanoparticles of gold, platinum, and various PtAu alloys has been carried out, while the influence of sorbitol has been investigated along with the effects of different KOH concentrations, charge-transfer resistance, scan rates, and temperature when performing the sorbitol oxidation reaction (SOR). The results provided further support for the notion that PtAu catalysts can positively affect SOR efficiency in addition to facilitating the generation of shorter-chain byproducts due to enhanced electron transfer dynamics. In another study, Torres-Pacheco *et al.* (Torres-Pacheco *et al*., 2022) examined bimetallic palladium-gold (Pd_xAu_y/C) catalysts and their effects upon sorbitol electro-oxidation when using alkaline media. While the compositions and particle sizes are similar, the catalytic activity is primarily affected by bimetallic interactions, in turn shaping the electronic and structural properties. A number of catalysts were tested, with the best performance reported for $Pd_{60}Au_{40}$/C and $Pd_{40}Au_{60}$/C, while the greatest current density was achieved by $Pd_{60}Au_{40}$/C, significantly outperforming monometallic Pd or Au. These outcomes clearly demonstrate the superior stability and activity of Pd-based bimetallic catalysts and confirm the possibility of employing them in fuel cells where sorbitol is involved.

This study places particular emphasis upon the polyalcohol type used. One type which is commonly employed in sugar substitutes to make chewing gum or mints is xylitol. The advantage of using xylitol instead of sucrose is that comparable amounts have 33% fewer calories, while it offers low toxicity and 1 gram of xylitol contains 2.4 kcal. The electrochemical characteristics of xylitol solutions still require further study, although it is known that the oxidation reaction takes place at the anode, as is the case for glucose or glycerol. Furthermore, xylitol solutions are able to donate electrons which feed the system with electricity through metal catalysts such as Pd/CNTs (Kannan *et al.*, 2016). The production of xylitol can be achieved through a variety of procedures. This study sought to examine the potential for utilizing xylitol solution as a fuel by examining how the different catalysts influence the reduction reaction electrochemistry occurring at the cathode of alkaline fuel cells.

2. Materials and methods

2.1 Synthesis of catalysts

2.1.1 Catalyst where the cathode is 20 wt% FeCo/C

Synthesis of the catalyst 20 wt% FeCo/C followed a process whereby 1.42 g of iron (II) chloride tetrahydrate ($FeCl_2{\cdot}4H_2O$) (Merck) along with 0.88 g of cobalt (II) chloride hexahydrate ($CoCl_2{\cdot}6H_2O$) (Merck) were initially dissolved in 50 mL of DI water, followed by agitation for 24 hours using magnetic stirrers. A 2 M NaOH solution was used alongside 0.3 g of sodium borohydride ($NaBH_4$) (Merck) to adjust the pH value to 9. A mixture was then produced comprising the catalyst, 3.2 g of Vulcan XC-72R carbon (Cabot Company), and FeCo, followed by the addition of deionized water. This solution was mixed for a further 24 hours using magnetic stirrers, before filtering the sediment and rinsing it repeatedly in deionized water. The final product was then allowed to dry for a period of 24 hours at a temperature of 80°C.

2.1.2 Catalyst where the cathode is 20 wt% AgFeCo/C

Preparation of the 20 wt% catalyst involved the use of AgFeCo/C along with 0.42 g of silver nitrate ($AgNO_3$) (Merck), 0.59 g of cobalt(II) chloride hexahydrate ($CoCl_2 \cdot 6H_2O$) (Merck), and 0.95 g of iron(II) chloride tetrahydrate ($FeCl_2 \cdot 4H_2O$) (Merck), to form a solution in 50 mL of DI water. The resulting mixture underwent agitation for 24 hours using magnetic stirrers. A 2 M NaOH solution was used alongside 0.5 g of sodium borohydride ($NaBH_4$) (Merck) to adjust the pH value to 9, and further agitation followed constantly for 24 hours. A mixture was then produced comprising the catalyst, 3.2 g of Vulcan XC-72R carbon (Cabot Company), and AgFeCo, followed by the addition of deionized water. This solution was mixed for a further 24 hours using magnetic stirrers, before filtering the sediment and rinsing it repeatedly in deionized water. The final product then underwent drying for 24 hours at a temperature of 80°C.

2.1.3 Catalyst where the anode is 20 wt% Pd/C

Synthesis of the 20 wt% catalyst made use of Pd/C along with 1.33 g of palladium (II) chloride ($PdCl_2$) (Merck) to produce a solution in 50 mL of DI water. The resulting mixture underwent agitation for 24 hours using magnetic stirrers. A 2 M NaOH solution was used alongside 0.3 g of sodium borohydride ($NaBH_4$) (Merck) to adjust the pH value to 11. Further agitation for 30 minutes followed, before filtering the sediment and repeatedly rinsing it in deionized water. The material produced was then dried for 24 hours at 80°C, whereupon the catalyst was added to 3.2 g of Vulcan XC-72R carbon (Cabot Company) and the Pd compound, followed by the addition of 50 mL of deionized water. This solution was mixed for a further 24 hours using magnetic stirrers, before filtering the sediment and rinsing it repeatedly in deionized water. Drying of the final product then took place for 24 hours at a temperature of 80°C.

2.2 Catalyst ink preparation

For the purposes of experimentation, a 0.2 w/v catalyst solution was prepared. This required the mixing of 0.01 g of the catalyst with 3.5 mL of isopropanol (Merck) and 1.5 mL of deionized water. This resulting mixture was then subjected to ultrasonication.

2.3 Working electrode preparation

Alumina powder of particle size 0.5 µm was used to clean the working electrode, which was then wiped carefully using ethanol before the addition of 1.5 µL of 5 wt% Nafion solution. The resulting mixture was allowed to stand for around 1 minute, by which time the Nafion solution was dehydrated. Finally, 5 µL of catalyst solution was introduced before allowing the mixture to stand for 24 hours. Cyclic voltammetry was then carried out for analysis purposes.

2.4 Catalyst electrochemical characterization

Cyclic voltammetry provided useful insights for the researchers concerning the effects of electrocatalysts when xylitol fuel underwent oxidation and reduction reactions in alkaline conditions (KOH). The main parameters comprised scan rates of 50 mV/s and 10 mV/s along with a potential range of -1.2 V to 1.2 V. To conduct the experiments, the setup made use of a nitrogen-saturated 0.1 M KOH solution along with a catalytic working electrode linked to a potentiometer, a silver chloride reference electrode, and a platinum counter electrode. The xylitol solutions, which were produced under alkaline conditions (KOH), had a range of concentrations from 0.1 M up to 0.5 M. These solutions were then introduced to 50 mL of the 0.1 M KOH, in alignment with the results of the initial study pertaining to alkaline solutions.

3. Results and Discussion

3.1 Physical attributes of the catalyst

3.1.1 STEM and EDS analysis

The surface morphology of the FeCo/C, AgFeCo/C, and Pd/C catalysts was evaluated through the use of STEM (scanning transmission electron microscopy), with the outcomes presented in Figure 1. It is apparent from the micrographs that the catalyst composition involves spherical metal particles which show a random distribution throughout the carbon support, creating a high degree of porosity and a large surface area. These qualities are particularly beneficial in promoting

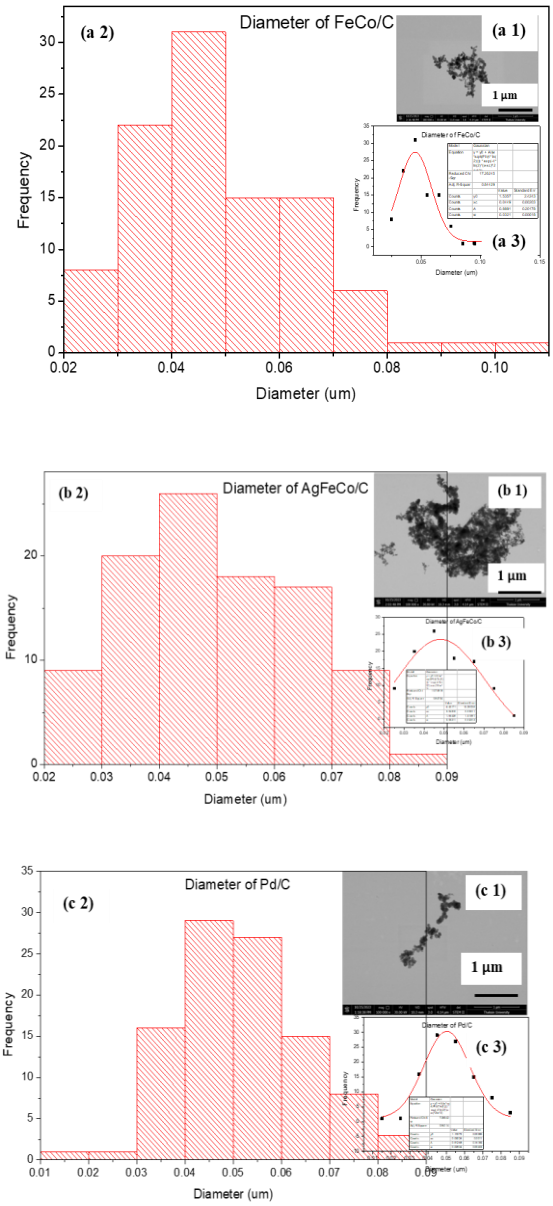

Fig. 1 STEM images showing the surface characteristics of the cathode and anode catalysts: (a1) FeCo/C, (b1) AgFeCo/C and (c1) Pd/C and size distributions of (a2, a3) FeCo/C, (b2, b3) AgFeCo/C and (c2, c3) Pd/C

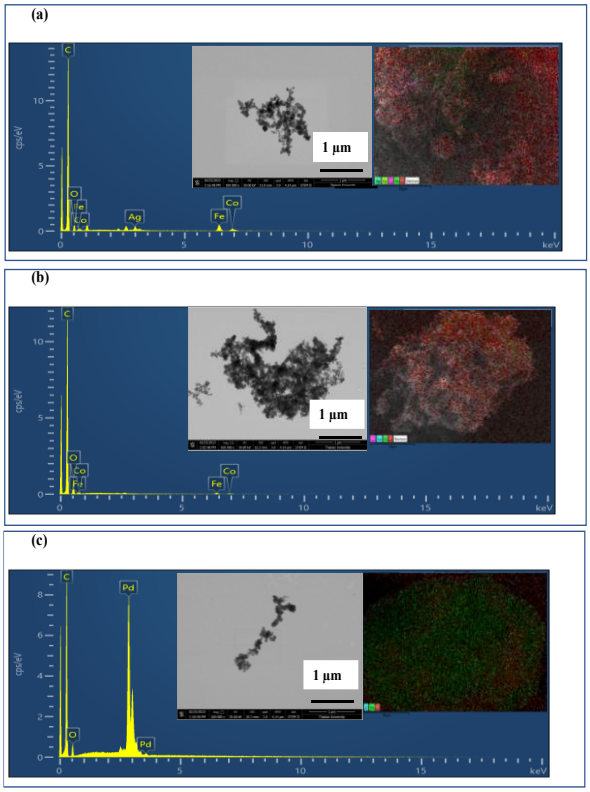

Fig. 2 STEM images, EDS, and EDS maps showing the elemental contents of the cathode and anode catalysts: (a) FeCo/C, (b)AgFeCo/C, and (c) Pd/C

catalysis (Masjod *et al.*, 2020). While the resolution achieved by SEM (scanning electron microscopy) is insufficient to permit accurate measurements of particle size, it is possible to assess both the presence and distribution of metal particles upon the surface through consideration of the scattering of electrons (Suwanraksa *et al.*, 2022). Further compositional analysis using energy-dispersive X-ray spectroscopy (EDS) mapping, shown in Figure 2, confirmed a relatively uniform dispersion of metal nanoparticles across the carbon substrate for all catalyst types. This uniformity is critical for optimizing catalytic performance, as the distribution and density of active metal sites directly influence electrochemical reactivity. Nevertheless, as detailed in Table 1, the actual surface metal content observed was lower than the theoretical amount calculated during catalyst synthesis, suggesting potential losses during preparation or limitations in metal incorporation efficiency. This discrepancy demonstrates the value of accurate metal quantification and dispersion analysis in catalyst design and optimization.

3.1.2 XRF analysis

To accurately analyze the metal content that adheres to the surface and diffuses into the deeper pores of the carbon support material (XC-72R), further investigation using X-ray fluorescence (XRF) is necessary. Unlike the EDS technique, which primarily detects surface-level elements, XRF provides a more comprehensive analysis by penetrating deeper into the porous structure of the support material and quantifying the elemental composition more precisely. As shown in Table 1, XRF analysis offers the percentage of metal particles relative to the total elements present on the catalyst surface, enabling a more accurate assessment of metal loading. The results for each catalyst type indicate that the ratio of metal to carbon closely aligns with the theoretical values calculated during the catalyst preparation stage, thereby confirming the efficiency and consistency of the metal incorporation process across different catalyst formulations. This finding indicates the importance of using complementary analytical techniques, such as XRF, to ensure accurate characterization of catalyst materials, particularly when evaluating metal dispersion within highly porous carbon supports.

3.1.3 X-ray diffraction (XRD) patterns of the cathode and anode catalysts

Fig. 3 shows the X-ray diffraction (XRD) patterns of the catalysts, cathode, and anode. The spectral lines of the AgFeCo/C and FeCo/C catalysts clearly showed Ag metal peaks at 2-theta positions of 38.12, 44.31, 64.46, 77.41, and 81.56 degrees, corresponding to patterns of (111), (200), (220), (311), and (222), respectively (JCPDS card no. 01071 3762), which indicates the presence of Ag metal particles with face-centered cubic (fcc) structures (Agasti *et al.* 2014). Fe_3O_4 metal peaks clearly appeared at 2-theta positions of 19.30, 30.09, 35.45, 43.08, 53.42, 56.97, 62.56, and 81.91 degrees, corresponding to patterns of (111), (220), (311), (400), (422), (511), (440), and (222) (JCPDS card no. 01-080-6402), which indicates the presence of Fe_3O_4 metal particles with spinel cube (Silva *et al.* 2013) structures, and Co_3O_4 metal peaks appeared at 2-theta positions of 30.09, 56.97, and 77.41 degrees, corresponding to patterns of (220) and (422) (JCPDS card no. 42-1467), indicating the presence of Co_3O_4 metal particles with spinel cubic structures (Chen *et al.* 2015).

For the FeCo/C catalyst, the Fe_3O_4 metal peak appeared at 2-theta positions of 31.05 and 45.01, and the Co_3O_4 metal peak at the 2-theta position was the same as the Fe_3O_4 metal peak, showing the same patterns. (220) and (400) (JCPDS card no. 01-080-6402) (JCPDS card no. 42-1467), respectively (Silva *et al.* 2013), which indicates the presence of Fe_3O_4 and Co_3O_4 metal particles within the structure of the same spinel cube (Chen *et al.* 2015) and depicts the X-ray diffraction (XRD) patterns of the catalysts, cathode, and anode. The spectral lines of the Pd/C catalysts clearly showed Pd metal peaks at 2-theta positions of 40.12, 46.66, 68.13, 82.11, and 86.63 degrees, corresponding to the (111), (200), (220), (311), and (222) planes, respectively, which is consistent with standard data (JCPDS No. 01-087-0637) and indicates the presence of face-centered cubic (fcc) Pd metal particles (Filho *et al.* 2022).

Analysis of the AgFeCo/C, FeCo/C, and Pd/C catalyst XRD patterns showed clear crystalline phases along with

Table 1.
Theoretical percentage by weight analysis of the FeCo/C, AgFeCo/C, and Pd/C cathode and anode catalysts

Catalyst	The percent by weight analysis (EDS)	The percent by weight analysis (XRF)
Cathode catalyst	**(Ag : Fe : Co : C)**	**(Ag : Fe : Co : C)**
FeCo/C	0 : 1.25 : 0.67 : 77.17	0 : 12.98 : 7.44 : 76.90
AgFeCo/C	2.62 : 6.13 : 2.45 : 79.75	1.99 : 13.05 : 4.51 : 78.60
Anode catalyst	**(Pd : C)**	**(Pd : C)**
Pd/C	14.27 : 68.97	20.71 : 76.48

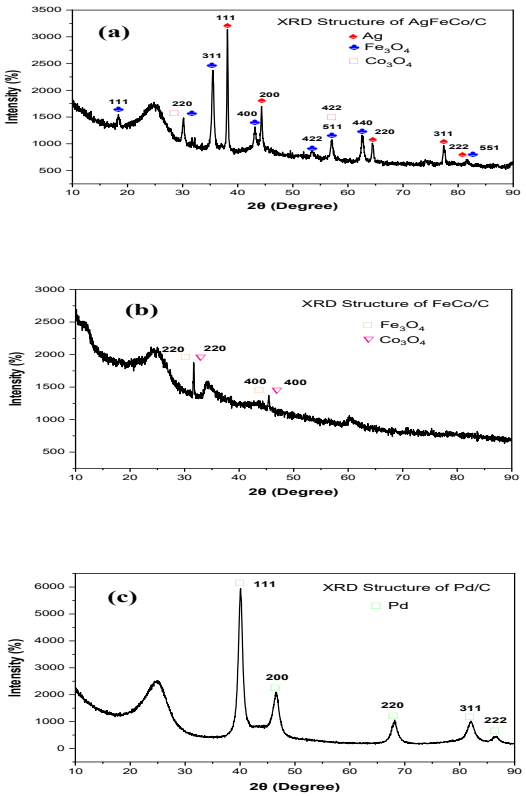

Fig. 3 X- ray diffraction patterns of the cathode and anode Catalysts: (a) FeCo/C, (b) AgFeCo/C, and (c) Pd/C

structural features which serve to determine the electrochemical behavior of these catalysts. For example, high crystallinity is indicated in the Pd/C sample by the appearance of sharp peaks which are very clearly defined. High crystallinity is usually associated with improved electrical conductivity and catalytic activity when electrochemical reactions take place. However, the AgFeCo/C and FeCo/C catalysts exhibit broader peaks which are typical of smaller crystallite sizes and indicate the possibility of amorphous or alloyed structures. The structural properties have a positive effect upon electrochemical performance in offering a larger number of active sites as well as promoting charge transfer. Furthermore, when different metals are incorporated, synergistic effects serve to alter the electronic structure of the surface of the catalyst, thus affecting the intermediate adsorption energies, and making the catalysis process more efficient. Accordingly, the structural characteristics observed via XRD analysis have a direct influence upon the reported electrochemical activity of the catalysts. In particular, crystallite size and alloying are important factors affecting both stability and activity (Zhong *et al.*, 2023; Zhiani *et al.*, 2018).

3.2 Electrochemical characterization of the catalyst

3.2.1 Electrochemical characteristics of the cathode catalyst

The study conducted cyclic voltammetry analysis of the FeCo/C and AgFeCo/C cathode catalysts in an alkaline solution at a concentration of 0.1 M. This trend can be seen when the current range was scanned. The reduction reaction peak of the catalyst appears in the potential range of approximately (-0.75) to (-0.30) V, indicating the formation of CoO_2 during the catalyst recovery process before the next scan cycle, as shown at position 1 in Equation (1). Additionally, the reduction reaction peak in the potential range of approximately -0.75 to -1.20 V corresponds to the electron absorption process due to the formation of $FeOOH^-$ and $CoOOH^-$ at position 2, as shown in Equations (2) and (3). After the addition of Ag, the subsequent scan revealed no $AgOH^-$ formation or reduction of AgO^- to accept electrons. This absence is due to FeO and CoO interfering with the reaction process.

The reaction equations of cobalt metal (Ding *et al.* 2010), which are based on a fuel using a glucose solution whose structure is similar to that of xylitol solution, explain the reaction mechanism of cobalt metal.

$$Co_3O_4 + OH^- + e^- \leftrightarrow 3CoOOH + H_2O \quad (1)$$
$$CoOOH + OH^- + e^- \leftrightarrow CoO_2 + H_2O \quad (2)$$
$$2CoO_2 + C_5H_{12}O_5 \text{ (xylitol)} \rightarrow 2CoOOH + C_5H_{10}O_5 \quad (3)$$

Under alkaline conditions, the $FeCo_2O_4$-catalyzed xylitol reaction begins with $FeCo_2O_4$ reacting with OH^- ions and water to produce Fe (III) and Co (III) intermediates ($FeOOH^-$ and $CoOOH^-$) on the electrode surface (Equation 4). Following this, xylitol is oxidized, with electrons directly transferring to these Fe (III) and Co (III) species, leading to their reduction to FeO and CoO (Equation 5).

The electron transfer process involving FeO and CoO is an electric current accumulator. Fe (III) and Co (III) are regenerated, as shown in Equation (6), which can further activate the catalytic reaction of $FeCo_2O_4$ for the reduction of xylitol, leading to the formation of only FeO and CoO. This process demonstrates a synergistic effect between Fe (III) and Co (III) (Dong *et al.* 2019).

The reaction equations of iron–cobalt metal, which are based on a fuel using a glucose solution whose structure is similar to that of xylitol solution, explain the reaction mechanism of iron–cobalt metal.

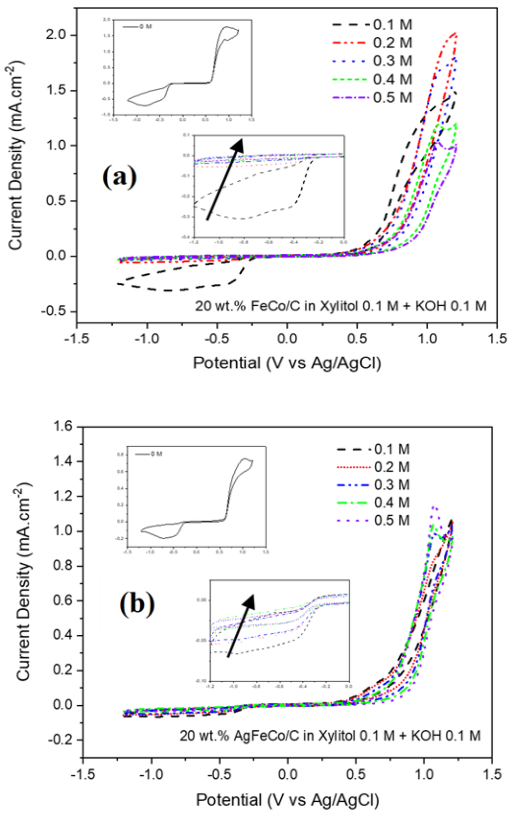

Fig. 4 Cyclic voltammograms of the cathode catalysts (a) FeCo/C and (b) AgFeCo/C in 0.1 M KOH solution doped with 0.1 to 0.5 M xylitol at a scan rate of 0.01 V/s

$FeCo_2O_4 + OH^- + e^- \rightarrow FeOOH + 2CoOOH + H_2O$ (4)
$FeOOH + CoOOH + xylitol \rightarrow FeO + CoO + xylitol$ oxidation products (5)
$FeO + CoO + 2e^- \rightarrow FeOOH + CoOOH + 2OH^-$ (6)

A 0.1 M KOH solution exhibited excellent catalytic performance. For FeCo/C, the highest current density of the reduction peak was -0.45 mA.cm^{-2} at -0.72 V. For the AgFeCo/C and FeCo/C catalysts, dilution with 0.1 to 0.5 M xylitol affected the reduction reaction, as shown in Figure 4. As cathode-side catalysts, AgFeCo/C and FeCo/C inherently resist oxidation, which is desirable for the cathode's required reduction reaction. However, increasing the xylitol concentration diminished the reduction reaction's efficiency. This reduction is attributed to non-conductive hydrocarbons that, at xylitol concentrations above 0.1 M, can disrupt electron transfer or block xylitol adsorption on the catalyst surface, thereby hindering the reduction reaction (Kannan *et al.,* 2016).

3.2.2 Electrochemical characteristics of the anode catalyst

Observations reveal two distinct oxidation reaction peaks upon diluting the sample with a xylitol solution ($C_5H_7(OH)_5$). These peaks occur during the forward scan, spanning potential ranges of -0.75 V to -0.25 V and -0.25 V to 0.25 V, suggesting the adsorption of xylitol molecules onto the metal's surface, as described in Equation (7).

$$Pd + (C_5H_7(OH)_5) \rightarrow Pd + (C_5H_7(OH)_5)\,ads \quad (7)$$

A reoxidation peak is observed in the case of a reverse scan within the potential range of (-0.25) to (-0.5) V. This peak is due to the formation of a Pd (II) oxide layer on the surface of the catalyst, which is the first step in oxide formation on the catalyst's metal surface (Suwanraksa *et al.* 2021). As the potential increases, the catalyst forms more metal oxides. In the reverse scan at a potential of -0.3 V, the reduction reaction of Pd (II) leads to further formation of a metal oxide, as shown in Equation 8.

$$Pd - O + H_2O + 2e^- \leftrightarrow Pd + 2OH^- \quad (8)$$

For the study of the oxidation of Pd/C catalysts, the oxidation reaction occurred in the voltage range of -0.5 V to 0.5 V (Figure 5). The highest oxidation site was 0.9 mA.cm^{-2} Pd/C (-0.09 V) at 0.1 M xylitol.

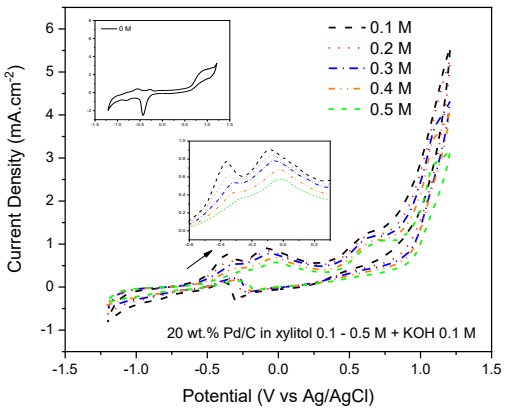

Fig. 5 Cyclic voltammogram of the anode catalyst Pd/C in 0.1M KOH solution doped with 0.1 to 0.5 M xylitol at a scan rate of 0.01 V/s

3.2.3 RDE (Rotating disk electrode) electrochemical characteristics

During the course of this research, the electrochemical characteristics of cathode catalysts were investigated in the context of the oxygen reduction reaction (ORR) in alkaline (KOH) electrolytes as well as xylitol-based electrolytes. The objective was to establish a deeper understanding of the mechanisms governing electron transfer as well as the kinetic parameters which affect the oxygen reduction reaction. The study focused upon electron transfer number assessment and evaluating both diffusion-limited and mass transport-limited current densities, since these are notable indicators of the effectiveness of catalysts along with the kinetics of the reactions. To investigate the performance of the AgFeCo/C and FeCo/C catalysts, cyclic voltammetry was carried out using a mixed electrolyte comprising 0.1 M KOH and 0.1 M xylitol. It was possible through the use of this dual-component electrolyte to analyze in greater detail the effects of polyalcohols such as xylitol upon the ORR under alkaline conditions. Cyclic voltammetry provided electrochemical data which was then utilized to determine the kinetic parameters, confirming that the electron transfer which takes place within the system tends to be limited by reaction kinetics instead of solely mass transport. These findings clearly demonstrate the necessity for additional catalyst structure and composition optimization. In general, the research provides useful insights concerning the electrochemical kinetics of the oxygen reduction reaction upon rotating disk electrodes, and this supports the ongoing development of fuel cell technologies.

On the basis of the equation of Koutecky- Levich, by drawing a graph showing the relationship between $1/j$ and $\omega^{-1/2}$, the slope of the graph is equal to $\left(\frac{1}{0.620nFAD^{2/3}\vartheta^{-1/6}C}\right)$, where n is the number of electrons transferred in the reduction of oxygen, F is Faraday's constant (96,485 C.mol^{-1}), A is the geometric surface area of the RDE (A = 0.196 cm^2), C_O is the bulk concentration of the oxygen, D is the diffusion coefficient of the oxygen, ν is the kinematic viscosity of the working electrolyte, C is the concentration of the electrolyte and ω is the angular rotation rate of the electrode (1600 rpm = 12.946 rad s^{-1}) (Koscher *et al.* 2004; Qiao *et al.* 2013; Chatenet *et al.*, 2009).

The y-intercept is equal to the y-intercept equal to $1/j_k$ mentioned earlier; one can determine the limiting current density of diffusion (j_d), the kinetic current density of the dynamics (j_k), and the number of electrons participating in the reaction (n) (Hunsom 2012; Prats *et al.* 2021).

According to the findings presented in Figure 6, the AgFeCo/C catalyst has a lower kinetic current density (j_k) than the FeCo/C catalyst. This result indicates that the oxygen reduction reaction is accelerated to a lesser extent by the same catalyst. Levich's study suggested that the electric current is proportional to $\omega^{-1/2}$, where ω is the angular velocity of the electrodes. However, at higher angular velocities, the curve deviates from a straight line, indicating that the reaction dynamics limit the electron transfer in the system, as shown in Figure 6. Therefore, a lower kinetic current density (j_k) for a catalyst implies that less electron transfer occurs in the system. For both the FeCo/C and AgFeCo/C catalysts, the average number of electrons (n) involved in the catalytic reaction was 2.41 and 3.45, respectively. The FeCo/C catalyst has a path lower than the 4-electron path, and the latter finding indicates that the oxygen reduction reaction proceeds via the electron pathway, producing a hydrogen peroxide intermediate that has a less negative impact on the catalyst's active area.

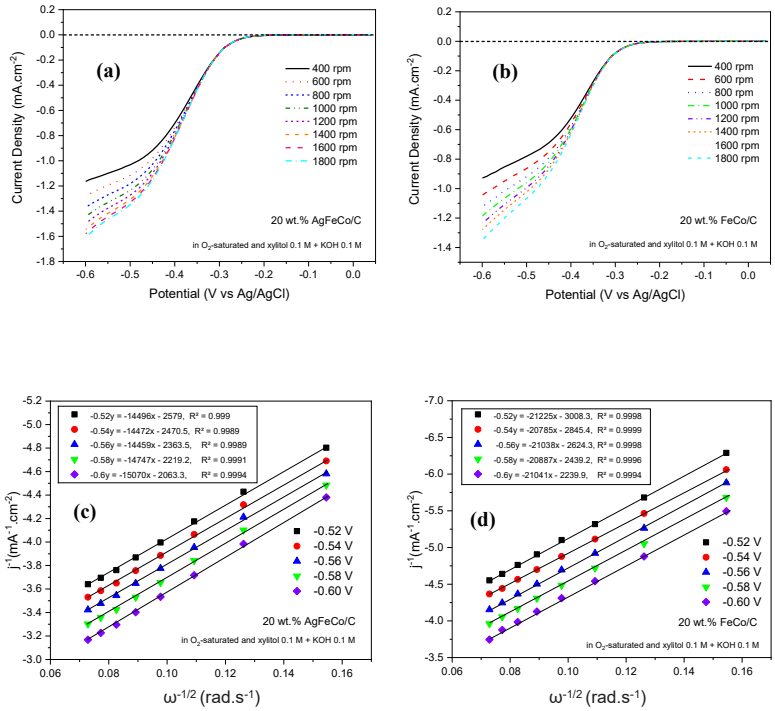

Fig. 6 Oxygen reduction reaction potential scan curves of (a) AgFeCo/C and (b) FeCo/C on a rotating disk electrode in O_2-saturated 0.1 M KOH at a sweep rate of 10 mV.s^{-1} (c) and (d) Koutecky–Levich plots of AgFeCo/C and FeCo/C

3.3 Performance of xylitol fuel cells via the electric potential difference measurement technique

As shown in Figure 7, the fuel cell configuration utilizing a Pd/C anode and an AgFeCo/C cathode achieved a voltage efficiency of 0.36 V under a load resistance of 2,000 ohms, corresponding to a power density of 0.129 W·m^{-2}. In comparison, a similar setup using a Pd/C anode paired with an FeCo/C cathode yielded a slightly lower voltage efficiency of 0.34 V and a corresponding power density of 0.112 W·m^{-2}. When subjected to thermal conditions (e.g., fire testing), the Pd/C–AgFeCo/C configuration demonstrated a 13.18% higher power output than its FeCo/C counterpart, primarily due to the inclusion of silver (Ag), a cost-effective, durable, and electrochemically stable metal. The superior performance of Ag-based catalysts can be attributed to their enhanced oxygen reduction reaction (ORR) kinetics in alkaline environments, where silver promotes more effective dissociation of O–O bonds while minimizing the formation of strong Ag–O_2 interactions. The observed behavior promotes enhanced electron transfer as well as catalytic activity, indicating the suitability of the AgFeCo/C catalyst for applications involving fuel cells. Furthermore, combining silver with inexpensive transition metals including cobalt (Co) or iron (Fe) leads to superior catalytic performance in addition to lowering the cost of production. This may prove valuable in developing scalable technologies in the field of low-cost fuel cells which offer greater levels of efficiency and effectiveness (Ashok *et al.*, 2018).

4. Conclusion

This study used STEM and EDS mapping to investigate the composition and morphology of cathode and anode catalysts for alkaline fuel cells. The analysis revealed that the prepared catalysts comprised very small particles densely distributed on

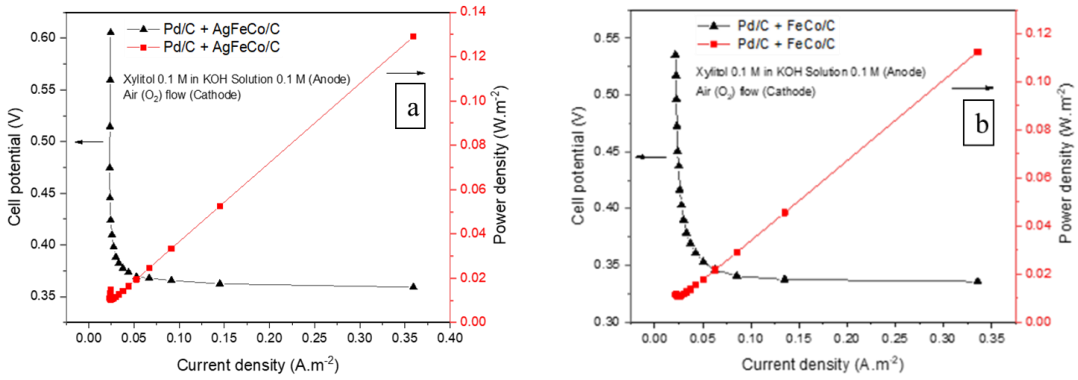

Fig. 7 Polarization and power density curves of a xylitol direct-fed alkaline fuel cell (a) Pd/C-AgFeCo/C catalysts and (b) Pd/C- FeCo/C

the carbon support surface. In the X-ray diffraction pattern of the cathode catalyst, the spectral lines of the Ag metal peak at the 2θ maximum position of 38.12 degrees displayed a pattern of 111, which indicates the presence of Ag metal particles with a face-centered cubic (fcc) structure. The Fe_3O_4 and Co_3O_4 metal peaks at the 2θ maximum positions of 35.45 and 30.09 degrees, respectively, displayed patterns of 311 and 220, indicating the presence of Fe_3O_4 and Co_3O_4 metal particles with spinel cubic structures. For the anode catalyst, the spectral line of the Pd metal peak at the 2θ maximum position of 40.12 degrees displayed a pattern of 111, indicating the presence of Pd metal particles with a face-centered cubic (fcc) structure. Electrocatalytic properties for xylitol oxidation were assessed via cyclic voltammetry (CV) across xylitol concentrations from 0.1 to 0.5 M in 0.1 M KOH (scan rate: 0.01 V. s^{-1}). FeCo/C and AgFeCo/C catalysts, suitable for the cathode due to their oxidation resistance, showed a reduced reaction efficiency with increasing xylitol concentration. In contrast, Pd/C catalysts excelled, achieving a peak oxidation current density of 0.9 $mA.cm^{-2}$ at -0.09 V with 0.1 M xylitol. The Pd/C-AgFeCo/C catalyst delivered the best fuel cell performance, with a current density of 0.36 $A.m^{-2}$ and a maximum power density of 0.129 $W.m^{-2}$.

Acknowledgments

This research was supported by Thailand Science Research and Innovation (TSRI), Thailand funded 2024.

Author Contributions: C.C.: conceptualization, investigation, funding acquisition, project administration, reviewing, and editing; B.Y.: methodology, reviewing and editing; S.I.: methodology, reviewing and editing; S.D.: investigation, methodology, writing an original draft, research design, and data analysis. All the authors have read and agreed to the published version of the manuscript.

Funding: This research was supported by Thailand Science Research and Innovation (TSRI), Thailand, which was funded in 2024.

Conflicts of Interest: The authors declare no conflicts of interest.

References

Agasti, N., & Kaushik, N.K. (2014). One pot synthesis of crystalline silver nanoparticles. *American Journal of Nanomaterials*, 2(1), 4-7. https://doi.org/10.12691/ajn-2-1-2

Ashok, A., Kumar, A., Matin, M.A., Tarlochan, F. (2018). Synthesis of highly efficient bifunctional Ag/Co_3O_4 catalyst for oxygen reduction and oxygen evolution reactions in alkaline medium. *ACS Omega*, 3(7), 7745–7756 https://doi.org/10.1021/acsomega.8b00799

Askari, M.B., Salarizadeh, P., & Bartolomeo, A.D. (2022). NiCo2O4-rGO/Pt as a robust nanocatalyst for sorbitol electrooxidation. *International Journal of Energy Research*, 46(5), 6745–6754. https://doi.org/10.1002/er.7614

Basu, D., & Basu, S. (2010). A study on direct glucose and fructose alkaline fuel cell. *Electrochimica Acta*, 55(20), 5775–5779. https://doi.org/10.1016/j.electacta.2010.05.016

Chatenet, M., Molina-Concha, M. B., El-Kissi, N., Parrour, G., Diard, J. P., (2009). Direct rotating ring-disk measurement of the sodium borohydride diffusion coefficient in sodium hydroxide solutions. *Electrochimica Acta*, 54, 4426-4435. https://doi.org/10.1016/j.electacta.2009.03.019

Chen, Y.H., Zhou, J.F., Mullarkey, D., Connell, R.O., Schmitt, W., Venkatesan, M., Coey, M., Zhang, H.Z. (2015). Synthesis, characterization and magnetic properties of ultrafine Co_3O_4 octahedra. *AIP Advances*, 5(8), 087122. https://doi.org/10.1063/1.4928494

Chutia, B., & Bharali, P. (2022). Oxygen deficient interfacial effect in CeO_2-modified Fe_2O_3/C for oxygen reduction reaction in alkaline electrolyte. *Catalysis Communications*, 164, 106432. https://doi.org/10.1016/j.catcom.2022.106432

Cruz-Reyes, I., Trujillo-Navarrete, B., García-Tapia, K., Salazar-Gastéluma, M.I., Paraguay-Delgado, F., & Félix-Navarro, R.M. (2020). Pd/MnO_2 as a bifunctional electrocatalyst for potential application in alkaline fuel cells.*Fuel*, 279, 118470.https://doi.org/10.1016/j.fuel.2020.118470

Daşdelen, Z., Özcan, A., & Özcan, A. (2021). Preparation of anode catalysts for sorbitol electrooxidation based on the nanocomposites of fumed silica, reduced graphene oxide and gold nanoparticles. *International Journal of Hydrogen Energy*, 46(55),28121-28133. https://doi.org/10.1016/j.ijhydene.2021.06.060

Dai, Y., Ding, J., Li, J., Li, Y., Zong, Y., Zhang, P., Wang, Z., & Liu, X. (2021). N, S and transition-metal co-doped graphene nanocomposites as high-performance catalyst for glucose oxidation in a direct glucose alkaline fuel cell. *Nanomaterials*, 11(1), 202. https://doi.org/10.3390/nano11010202

Ding, Y., Wang, Y., Su, L., Bellagamba, M., Zhang, H., & Leia, Y. (2010). Electrospun Co_3O_4 nanofibers for sensitive and selective glucose detection. *Biosensors and Bioelectronics*, 26(2), 542–548. https://doi.org/10.1016/j.bios.2010.07.050

Dong, F., Liu, X., Irfan, M., Yang, l., Li, S., Ding, J., Li, Y., Khan, I.U., & Zhang, P. (2019). Macaroon-like FeCo2O4 modified activated carbon anode for enhancing power generation in direct glucose fuel cell. *International Journal of Hydrogen Energy*, 44(16), 8178-8187. https://doi.org/10.1016/j.ijhydene.2019.02.031

Elsheikh, A., & McGregor, J. (2021). Synthesis and Characterization of PdAgNi/C Trimetallic Nanoparticles for Ethanol Electrooxidation. *Nanomaterials,* 11(9), 2244.. https://doi.org/10.3390/nano11092244

Ferriday T.B., & Middleton, P.H. (2021). Alkaline fuel cells: theory and application. *International Journal of Hydrogen Energy*, 46(35), 18489-18510.. https://doi.org/10.1016/j.ijhydene.2021.02.203

Filho, Y.F., Carvalho da Cruz, A.C., Pedicini, R., Salgado, J.R., Rodrigues, R.V., Luz, P.P., Garcia-Segura, S., & Josimar, R. (2022). PdAg/C Electrocatalysts Synthesized by Thermal Decomposition of Polymeric Precursors Improve Catalytic Activity for Ethanol Oxidation Reaction. *Catalysts,* 12(1), 96. https://doi.org/10.3390/catal12010096

Gao, M., Liu, X., Irfan, M., Shi, J., Wang, X., & Zhang, P. (2018). Nickle-cobalt composite catalyst-modified activated carbon anode for direct glucose alkaline fuel cell. *International Journal ofHydrogen Energy*, 43(3), 1805-1815. https://doi.org/10.1016/j.ijhydene.2017.11.114

Ghouri, Z.K., Barakat, N.A.M., Obaid, M., Lee, J.H., & Kim, H.Y.(2015). Co/CeO_2-decorated carbon nanofibers as effective on-precious electro-catalyst for fuel cells application in alkaline medium. *Ceramics International*, 41(2), 2271–2278. https://doi.org/10.1016/j.ceramint.2014.10.031

Ho, J.H., Li, Y., Dai, Y., Kim, T., Wang, J., Ren, J., Yun, H.S., & Liu, X. (2021). Ionothermal synthesis of N-doped carbon supported $CoMn_2O_4$ nanoparticles as ORR catalyst in direct glucose alkaline fuel cell. *International Journal of Hydrogen Energy*, 46, 20503-20515. https://doi.org/10.1016/j.ijhydene.2021.03.145

Hu, J., Lu, H., Li, M., Xiao, G., Li, M., Xiang, X., Lu, Z., & Qiao, Y. (2022). Cobalt valence modulating in CoOx incorporated carbon nanofiber for enhanced glucose electrooxidation. *Materials Reports: Energy*, 2(2), 100091. https://doi.org/10.1016/j.matre.2022.100091

Huang, J., Simons, P., Sunada, Y., Rupp, J., & Yagi, S. (2021). Pt-catalyzed d-glucose oxidation reactions for glucose fuel cells. *Journal of The Electrochemical Society*, 168, 064511. https://doi.org/10.1149/1945-7111/ac0949

Hunsom, M. (2012). PEM fuel and electrochemical analysis. Chulalongkorn University Press. Bangkok.

Kannan, R., Kim, A.R., Nahm, K.S., & Yoo, D.J. (2016). Facile instep synthesis of palladium nanoparticle/carbon@carbon nanotube

composites for electrooxidation of xylitol. Journal of Nanoscience and *Nanotechnology*, 16(3), 2587-2592. https://doi.org/10.1166/jnn.2016.10769

Koscher, G., Kordesh, K., (2004).Can refillable alkaline methanol-air systems replace metal-air cells?. *Journal of Power Sources*, 136, 215-219. https://doi.org/10.1016/j.jpowsour.2004.03.005

Liu, H., Yang, D.H., Wang, X.Y., Zhang, J., & Han, B.H. (2021). N-dope graphitic carbon shell-encapsulated FeCo alloy derived from metal-polyphenol network and melamine sponge for oxygen reduction, oxygen evolution, and hydrogen evolution reactions in alkaline media. *Journal of Colloid and Interface Science*, 581, 362-373.. https://doi.org/10.1016/j.jcis.2020.07.055

Liu, T. (2022). Glucose fuel cells and membranes: a brief overview and literature analysis. *Sustainability*, 14, 8376. https://doi.org/10.3390/su14148376

López-Coronel, A., Luis, J., Pacheco, T., Jennifer, A., Álvarez-López, A., Guerra-Balcázar, M., Álvarez-Contreras, L., & Arjona, A. N. (2020). Highly active PdNi bimetallic nanocubeselectrocatalysts for the ethylene glycol electro-oxidation in alkaline medium. *Applied Surface Science*, 530, 147210.https://doi.org/10.1016/j.apsusc.2020.147210

Masjod, P., Suwanraksa, K., & Chaiburi, C. (2020). Development of binary catalysts support for the electro-oxidation reaction enhancement of glycerol alkaline fuel cell. *ASEAN Journal of Scientific and Technological Reports (AJSTR)*, 23(2):55-64.

Matsuoka, K., Iriyama, Y., Abe, T., Matsuoka, M., & Ogumi, Z. (2005). Alkaline direct alcohol fuel cells using an anion exchange membrane. *Journal of Power Sources*, 150, 27-31. https://doi.org/10.1016/j.jpowsour.2005.02.020

Prats, H., Chan, K., (2021). The determination of the HOR/HER reaction mechanism from experimental kinetic data, *Physical Chemistry Chemical Physics*, 23, 27150. https://doi.org/10.1039/d1cp04134g

Qiao, J., Xu, L., Ding, L., Shi, P., Baker, R., Zhang, J., (2013). Effect of KOH concentration on the oxygen reduction kinetics catalyzed by heat-treated Co-Pyridine/C electrocatalysts. *International Journal of Electrochemical Science*, 8, 1189-1208. https://doi.org/10.1016/S1452-3981(23)14091-0

Silva, V.A.J., Andrade, P.L., Silva, M.P.C., Bustamante, A., Valladares, L., & Aguiar, J.A. (2013). Synthesis and characterization of Fe_3O_4 nanoparticles coated with fucan polysaccharides. *Journal of Magnetism and Magnetic Materials*, 343, 138-143.https://doi.org/10.1016/j.jmmm.2013.04.062

Suwanraksa, K., Chaiburi, C., & Bunyord, S. (2022). Efficiency of cathode catalyst between Ag/C and AgMnxOy/C for glucose membraneless alkaline fuel cell. *Journal of Applied Research on Science and Technology (JARST),* 21(2), 126-135.

Suwanraksa, K., Masjod, P., & Chaiburi, C. (2021). Bimetallic of Pd-CeOx/C electrocatalyst for electro-oxidation reaction ofxylitol fuels in alkaline solutions. *KKU Science Journal*, 49(2), 165-173.

Suzuki, T., Fujino, M., & Yamada, Y. (2023). Formation of a palladium catalyst layer using an anionic surfactant and subsequent fabrication of a glucose fuel cell. *Journal of Chemical Education*, 100(12), 4780−4785. https://doi.org/10.1021/acs.jchemed.3c00555

Torres-Pacheco, L.J., Leon-Rodriguez, A.D., Álvarez-Contreras, L., Guerra-Balcazar, M., & Arjona, N. (2020). Sorbitol electro-oxidation reaction on sub<10 nm PtAu bimetallic nanoparticles. *Electrochimica Acta*, 353, 136593. https://doi.org/10.1016/j.electacta.2020.136593

Torres-Pacheco, L.J., Leon-Rodriguez, A.D., Bañuelos, J.A., Álvarez-Contreras, L., Guerra-Balcázar, M., & Arjona, N. (2022). Electrocatalytic oxidation of sorbitol on PdxAuy/C bimetallic nanocatalysts. *Fuel*, 314, 122788. https://doi.org/10.1016/j.fuel.2021.122788

Kruusenberg, I., Matisen, L., Shah, Q., Kannan, A.M., & Tammeveski, K. (2012). Non-platinum cathode catalysts for alkaline Membrane fuel cells. *International Journal of Hydrogen Energy*, 37, 4406-4412. https://doi.org/10.1016/j.ijhydene.2011.11.143

Wang, Q., Chena, F., Liua, Y., Gebremariama, T.T., Wang, J., Anb, L., & Johnston, R.L. (2018). AgSn intermetallics as highly selectiveand active oxygen reduction electrocatalysts inmembraneless alkaline fuel cells. *Journal of Power Sources*, 404, 106-117. https://doi.org/10.1016/j.jpowsour.2018.10.013

Weiss, J., Zhang, H., & Zelenay, P. (2020). Recent progress in the durability of Fe-N-C oxygen reduction electrocatalysts for polymer electrolyte fuel cells. *Journal of Electroanalytical Chemistry*, 875, 114696. http://dx.doi.org/10.1016/j.jelechem.2020.114696

Xu, W., Zeng, R., Rebarchik, M., Posada-Borbon, A., Li, H., Pollock, C.J., Mavrikakis, M., & Abruna, H.D. (2024). Atomically dispersed Zn/Co−N−C as ORR electrocatalysts for alkaline fuel cells. *Journal of the American Chemical Society*, 146, 2593−2603. https://doi.org/10.1021/jacs.3c11355

Xu, X., Dong, X., Li, D., Qi, M., & Huang, H. (2023). ZIF-8-derived three-dimensional nitrogen-doped porous carbon as a Pt catalyst support for electrocatalytic oxidation of glucose in a glucose fuel cell. *ACS Applied Energy Materials*, 6, 2886−2896. https://doi.org/10.1021/acsaem.2c03833

Yang, J., Wang, J., Zhu, L., Gao, Q., Zeng, W., Wang, J., & Li, Y. (2018). Enhanced electrocatalytic activity of a hierarchical CeO_2@MnO_2 core-shell composite for oxygen reduction reaction. *Ceramics International*, 44(18), 23073-23079. https://doi.org/10.1016/j.ceramint.2018.09.111

Zhiani M., Abedini A. & Majidi S. (2018). Comparison of electro-catalytic activity of Fe-Ni-Co/C and Pd/C nanoparticles for glucose electro-oxidation in alkaline half-cell and direct glucose fuel cell. *Electrocatalysis*, 9, 735–743. https://doi.org/10.1007/s12678-018-0483-1

Zhong, J., Zhu, Z., Xu, Q., Peng L., Luo, K, & Yuan D. (2023). FeCo alloy nanoparticles supported on Co−N−C cubes derived from imidazolate frameworks as a bifunctional electrocatalyst for rechargeable zinc−air batteries. *Energy Fuels*, 37, 13489−13497.https://doi.org/10.1021/acs.energyfuels.3c02221